

# SCIENTIFIC REPORTS

OPEN

## Immobilization of Polyoxometalate in the Metal-Organic Framework rht-MOF-1: Towards a Highly Effective Heterogeneous Catalyst and Dye Scavenger

Received: 29 January 2016

Accepted: 18 April 2016

Published: 09 May 2016

Jing-Wen Sun<sup>1</sup>, Peng-Fei Yan<sup>1</sup>, Guang-Hui An<sup>1</sup>, Jing-Quan Sha<sup>2</sup>, Guang-Ming Li<sup>1</sup> & Guo-Yu Yang<sup>3</sup>

A series of three remarkable complexes  $[\text{P}Mo_{12}O_{40}]@[\text{Cu}_6\text{O}(\text{TZI})_3(\text{H}_2\text{O})_9]_4 \cdot \text{OH} \cdot 31\text{H}_2\text{O}$  ( $\text{H}_3\text{TZI}$  = 5-tetrazolyisophthalic acid; denoted as HLJU-1, HLJU = Heilongjiang University),  $[\text{Si}Mo_{12}O_{40}]@[\text{Cu}_6\text{O}(\text{TZI})_3(\text{H}_2\text{O})_9]_4 \cdot 32\text{H}_2\text{O}$  (denoted as HLJU-2), and  $[\text{PW}_{12}O_{40}]@[\text{Cu}_6\text{O}(\text{TZI})_3(\text{H}_2\text{O})_9]_4 \cdot \text{OH} \cdot 31\text{H}_2\text{O}$  (denoted as HLJU-3) have been isolated by using simple one-step solvothermal reaction of copper chloride, 5-tetrazolyisophthalic acid ( $\text{H}_3\text{TZI}$ ), and various Keggin-type polyoxometalates (POMs), respectively. Crystal analysis of HLJU 1–3 reveals that Keggin-type polyoxoanions have been fitted snugly in the cages of rht-MOF-1 (MOF: metal–organic framework) with large cell volume in a range of 87968–88800 Å<sup>3</sup> and large pore volume of about 68%. HLJU 1–3 exhibit unique catalytic selectivity and reactivity in the oxidation of alkylbenzene with environmental benign oxidant under mild condition in aqueous phase as well as the uptake capacity towards organic pollutants in aqueous solution.

Polyoxometalates (POMs), as a species of significant metal oxide clusters with high negative charge and abundant topologies, have been employed in many research fields, such as catalysis, optics, magnetism, and biological medicine<sup>1–10</sup>. Particularly, POMs-catalyzed oxidation reactions are garnering increasing attention although it is limited by their low specific surface area and low stability<sup>11</sup>. Nevertheless, immobilizing POMs in porous solid materials, such as silica and activated carbon is a promising approach to stabilize POMs and optimize their catalytic performance<sup>12–15</sup>. Among these solid supports, porous metal-organic frameworks (MOFs) offer significant advantages of high surface area and porosity over the traditional solid supports<sup>16–29</sup>. Recently, several POMs have been encapsulated into several known MOFs. The resulted POM@MOFs have been applied to alkene epoxidation, oxidative desulfurization, aerobic decontamination, asymmetric dihydroxylation of olefins, and so on<sup>30–38</sup>. Among the reported POM@MOFs, POM@MIL-101 series have been the most investigated because of their large surface areas as well as unique chemical stability<sup>39–44</sup>. In addition to the POM@MIL-101, the POM@HKUST-1 series have been as well intensively studied that display unique catalytic selectivity and conversion in the oxidation of the mercaptans to disulfides and hydrolysis of esters<sup>45,46</sup>. Nevertheless, the current studies of POM@MOFs are mostly focused on MIL-101 and HKUST-1<sup>47–50</sup>. It remains great challenge to the immobilization of POMs into MOFs towards diverse structures and multifunctionalities. It is known that the rht-MOF-1 is highly porous with large surface area and possess a high concentration of open metal sites (OMSs). It contains four types of cage: cuboid (~5.9 Å), rhombitruncated cuboctahedral (~11.6 Å), β-cage like (~12.1 Å), and α-cage like (~20.2 Å) accessible through microporous quadrature windows (~6 Å), which is a potential host framework to encapsulate POMs that may be applied as catalysts<sup>51,52</sup>. Therefore, attempt of immobilizing the POMs into rht-MOF-1

<sup>1</sup>Key Laboratory of Functional Inorganic Material Chemistry Ministry of Education of the People's Republic of China, Heilongjiang University, Harbin, 150080, China. <sup>2</sup>School of Pharmacy, Jiamusi University, Jiamusi, 154007, China.

<sup>3</sup>Key Laboratory of Cluster Science Ministry of Education of the People's Republic of China, Beijing Institute of Technology, Beijing, 100081, China. Correspondence and requests for materials should be addressed to P.-F.Y. (email: yanpf@vip.sina.com) or G.-M.L. (email: gmli\_2000@163.com) or G.-Y.Y. (email: ygy@bit.edu.cn)

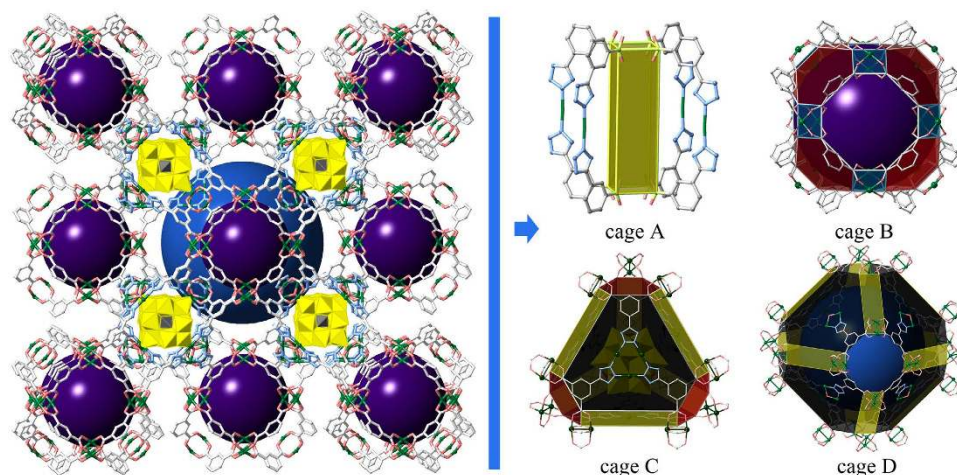


**Figure 1.** Ball/stick/polyhedral representations of four types of cages, (A–D) in HLJU-1. Color code: Cu, green; N, blue; O, pink; POM, yellow. All H atoms and solvent molecules are omitted for clarity.

was conducted by reactions of rht-MOF-1 with  $\text{H}_3\text{PMo}_{12}\text{O}_{40}$ ,  $\text{H}_4\text{SiMo}_{12}\text{O}_{40}$ , and  $\text{H}_3\text{PW}_{12}\text{O}_{40}$  in DMF and water, respectively. As a result, a series of three POM@MOFs,  $[\text{PMo}_{12}\text{O}_{40}]@[\text{Cu}_6\text{O}(\text{TZI})_3(\text{H}_2\text{O})_9]_4 \cdot \text{OH} \cdot 31\text{H}_2\text{O}$  (HLJU-1),  $[\text{SiMo}_{12}\text{O}_{40}]@[\text{Cu}_6\text{O}(\text{TZI})_3(\text{H}_2\text{O})_9]_4 \cdot 32\text{H}_2\text{O}$  (HLJU-2), and  $[\text{PW}_{12}\text{O}_{40}]@[\text{Cu}_6\text{O}(\text{TZI})_3(\text{H}_2\text{O})_6]_4 \cdot \text{OH} \cdot 31\text{H}_2\text{O}$  (HLJU-3) have been isolated. X-ray structure analyses indicate that the Keggin-type POMs are incorporated into the cages of rht-MOF-1. Catalytic experiments reveal that HLJU 1–3 exhibit unique catalytic selectivity and reactivity in the oxidation of alkylbenzene under mild condition with environmental benign oxidant in aqueous phase as well as the uptake capacity towards organic pollutants in aqueous solution.

## Results and Discussion

X-ray diffraction analysis reveals that HLJU 1–3 are isomorphous crystallizing in a highly symmetric space group of  $Fm\bar{3}m$  with large cell volume in the range of 87968–88800 Å<sup>3</sup>. The Keggin-type POMs ( $\text{H}_3\text{PMo}_{12}\text{O}_{40}$ ,  $\text{H}_4\text{SiMo}_{12}\text{O}_{40}$ , and  $\text{H}_3\text{PW}_{12}\text{O}_{40}$ ) have been first introduced into an open porous system as guests, respectively. The paddle-wheel unit  $\text{Cu}_2$ -clusters and triangular inorganic  $\text{Cu}_3$ -clusters are connected through the TZI ligands forming a three-dimensional cubic network. Notably, the host framework of HLJU 1–3 is isostructural with the famous complex rht-MOF-1<sup>52</sup>, indicating that *in situ* preparation of rht-MOF-1 is possible in a mixed solvent of DMF and distilled water in contrast in pure DMF. In a typical structure of HLJU-1, the asymmetric unit of HLJU-1 is of 3 Cu(II) cations, 1/2 triply deprotonated TZI ligand, and 1/12  $[\text{PMo}_{12}\text{O}_{40}]^{3-}$  polyoxoanion (abbreviated as  $\text{PMo}_{12}$ ) (Figure S1). The  $\text{PMo}_{12}$  polyoxoanion exhibits the well-known  $\alpha$ -Keggin configuration, consisting of a central  $\text{PO}_4$  tetrahedron and four corner-sharing triad  $\{\text{Mo}_3\text{O}_{13}\}$  clusters. There are three crystallographically independent Cu(II) cations in the structure. Both Cu1 and Cu2 cations adopt the tetragonal pyramid geometry, coordinated by five oxygen atoms, four oxygen atoms from four TZI ligands and one oxygen atom from axial water molecule. The Cu3 cation is five-coordinated in a trigonal bipyramidal coordination geometry, achieved by three oxygen atoms from three coordinated water molecules and two nitrogen atoms from two coordinated TZI ligands (Figure S2). The TZI ligand is six-coordinated in the hexagonal coordination geometry, achieved by six Cu(II) cations (Figure S3). As a result, the Cu1 and Cu2 cations form a paddle-wheel unit  $\text{Cu}_2$ -cluster ( $\text{Cu}_2(\text{O}_2\text{CR})_4$ ), and three Cu3 cations form a trinuclear cluster ( $\text{Cu}_3\text{O}(\text{N}_4\text{CR})_3$ ) (Figure S4).

There are four types of cages (A, B, C and D) with diameters of ca. 5.9, 11.6, 12.1 and 20.2 Å, accessible through the windows for ca. 5.9, 10.1, 7.1 and 8.2 Å, respectively (Fig. 1). Notably, only one of the four cages is occupied by a POM polyoxoanion, while the other filled by solvent molecules. Particularly, Cage A displays a cuboid shape which is constructed by two paddle-wheel unit  $\text{Cu}_2$ -clusters and four  $\text{Cu}(\text{N}_4\text{CR})_2$  edges (Figure S5). Cage B provides a rhombitruncated cuboctahedron in which the unit  $\text{Cu}_2(\text{O}_2\text{CR})_4$  constructs the twelve square, eight hexagonal and six octagonal planes, and carbon atoms of  $\text{Cu}_2(\text{O}_2\text{CR})_4$  locate on the 48 vertices (Figure S6). Obviously, the relative small diameters of cage A and cage B are not able to encapsulate the Keggin polyoxoanions (~10.5 Å). However, cage C, filling with the Keggin polyoxoanions, is of a  $\beta$ -cage like shape constructed by four large  $[\text{Cu}_3\text{O}(\text{N}_4\text{CR})_3]_3$  hexagon, four small  $[\text{Cu}_2(\text{O}_2\text{CR})_3]$  hexagon, and six  $\text{Cu}_2[\text{Cu}_2(\text{TZI})_2]_2$  rectangle, in which the carbon atoms of  $\text{Cu}_2(\text{O}_2\text{CR})_4$  locate on the 24 vertices (Figure S7). While, cage D with  $\alpha$ -cage like shape is assembled by eight large  $[\text{Cu}_3\text{O}(\text{N}_4\text{CR})_3]_3$  hexagon, six  $[\text{Cu}_2(\text{O}_2\text{CR})_4]$  octagon and twelve  $\text{Cu}_2[\text{Cu}_2(\text{TZI})_2]_2$  rectangle (Figure S8). On the basis of the very large cavity, the cage D is as well not suitable to encapsulate the Keggin polyoxoanions due to the weak interaction between the framework and POMs. The overall structure of HLJU-1 can be abbreviated as the *lta* topology (Fig. 2). The total solvent-accessible volume for HLJU 1–3 was estimated to be ~68% (~75% for rht-MOF-1) by summing voxels more than 1.2 Å away from the framework using PLATON software<sup>53–55</sup>. Strikingly, the pores are connected in nonlinear channels and facilitate reactant access and product departure. Each encapsulated POM can be accessed via eight adjacent pores. To the best of our knowledge, the verified structure of HLJU 1–3 is the second type of porous POM@MOF defined by crystal structure after

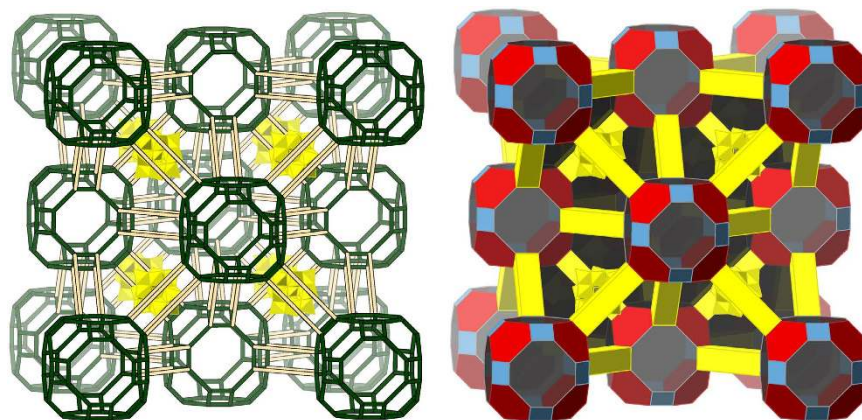


**Figure 2.** 3D HLJU-1 frameworks with *lta* topology. The MOF and POM polyoxoanions are represented by wireframe and polyhedral models.

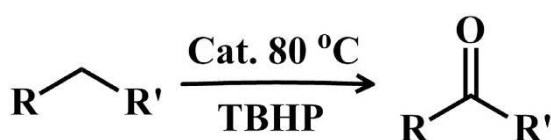


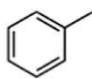
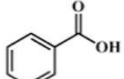
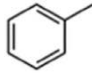
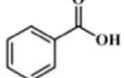
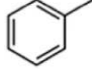
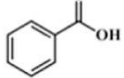
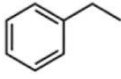
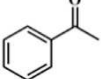
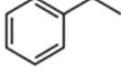
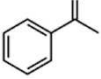
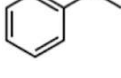
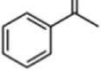
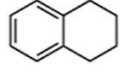
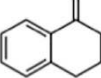
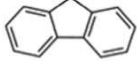
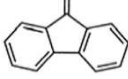
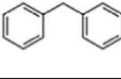
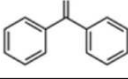
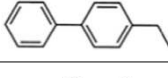
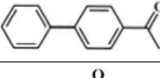
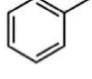
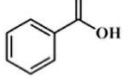
**Figure 3.** The reaction of alkylbenzenes with TBHP yielding corresponding Phenyl Ketones.

POM@HKUST-1 series. The electron paramagnetic resonance (EPR) of HLJU 1–3 exhibited the characteristic signal of Cu(II) with  $g = 2.12$  (Figure S11).

Since HLJU 1–3 contain catalytically active components of POMs and Cu<sup>II</sup>-MOF, it is encouraged to evaluate the catalytic ability of HLJU 1–3 in the oxidation reaction of alkylbenzene (Fig. 3). First of all, the contrast test of the catalytic activity among HLJU–1, rht-MOF-1 and (NBu<sub>4</sub>)<sub>3</sub>PMo<sub>12</sub>O<sub>40</sub> have been performed in the methylbenzene oxidation, respectively (Table 1, entries 1–3). GC–MS analysis showed that HLJU-1 exhibits the best conversion of 99% and single selectivity of benzoic acid (Table 1, entry 1), proving that the insertion of the POM into MOFs significantly enhanced the selectivity and reactivity for the oxidation reaction of alkylbenzene. Further contrast experiments of catalytic activity on oxidation of ethylbenzene reveal that HLJU-1 readily afforded acetophenone in the highest yield of 81% among HLJU 1–3 (Table 1, entry 4–6). The catalytic activity clearly indicates the difference of the POM polyoxoanions among HLJU 1–3, which is consistent with known sequence of [PMo<sub>12</sub>O<sub>40</sub>]<sup>3-</sup> > [PW<sub>12</sub>O<sub>40</sub>]<sup>3-</sup> > [SiMo<sub>12</sub>O<sub>40</sub>]<sup>4-</sup><sup>56</sup>. To investigate the effect of the size of the substrate on the catalytic conversions and selectivity, several substrates of alkylbenzene have been employed in the catalytic reactions by HLJU-1. As a result, (Table 1, entries 7–10) the catalytic conversions decrease along with the size increase of the alkylbenzenes, which is attributed to that the reactions may occur only on the solid surfaces. To further identify the catalytic sites of the alkylbenzene (e.g., on the crystal surfaces or in the open channels), the reaction time was extended to 36 h. The conversions of oxidation reaction reveal that the smallest ethylbenzene and the largest 4-ethylbiphenyl were not obvious increased along with the reaction time increase (8% and 12%, respectively).

However, the medium size of tetrahydronaphthalene, fluorene, and biphenyl methane exhibits a remarkable increase (23%, 21% and 16%, respectively) (Fig. 4). Thus, the core relationship between reaction rate and steric effect suggests that ethylbenzene can be diffused through the pores and touched the inner POM polyoxoanions. In contrast, tetrahydronaphthalene, fluorene, and biphenyl methane with larger steric effect are not diffused through the pores. They may absorb onto the surface pore containing Keggin complexes, leading to lower reaction rate. It should be noticed that the different catalytic conversions among the similar steric effect of fluorine, biphenyl methane, and 4-ethylbiphenyl may result from the activation of their benzene rings. The phenyl group would activate the adjacent C<sub>sp<sup>3</sup></sub>-H of benzyl group for the oxidation reactions. Thus, the fluorene and biphenyl methane with two phenyl groups possess the high conversion and reaction rate. Strikingly, HLJU-1 is recyclable up to at least the 5th cycle without losing its reactivity and selectivity under the reaction conditions. The recycled catalyst can be reused for these reactions after simple filtration, washing with acetonitrile, and drying. The PXRD patterns of HLJU-1 remain almost unchanged before and after the catalytic reactions, indicating the high stability and immobility of HLJU-1 (Figure S17).

We monitored the accessibility of the open channels to several substrate molecules and TBHP oxidant by <sup>1</sup>H NMR and GC-MS (see the SI for details). The NMR spectrum is clearly indicative of pore accessibility to ethylbenzene molecules and TBHP. A more quantitative analysis was conducted by GC–MS, from which uptake amounts of 16.9 wt % (for ethylbenzene) and 18.2 wt % (for TBHP) were obtained. On the contrary, no detectable amount was observed by <sup>1</sup>H NMR analysis for larger substrate molecules such as tetrahydronaphthalene, fluorene, and biphenyl methane under the same experimental conditions. These combined results suggest that the Cu(II) sites in the channel walls and POM polyanions in voids are indeed reachable by substrates of relatively

Entry	Substrate	Product	Catalyst	Conv. (%) <sup>b</sup>	Select. (%) <sup>b</sup>
1			HLJU-1	99	99
2			rht-MOF-1	64	81
3			(NBu <sub>3</sub> ) <sub>3</sub> [PMo <sub>12</sub> O <sub>40</sub> ]	trace	–
4			HLJU-1	81	89
5			HLJU-2	72	91
6			HLJU-3	75	92
7			HLJU-1	66	77
8			HLJU-1	65	99
9			HLJU-1	65	99
10			HLJU-1	54	99
11			HLJU-1	73	83 <sup>c</sup>

**Table 1. Oxidation of Alkylbenzenes to Phenyl Ketones Catalyzed by POM–MOFs<sup>a</sup>.** <sup>a</sup>Alkylbenzene (1 mmol), TBHP (5 mmol), and catalyst (0.005 mmol) were stirred at 80 °C for 12 h. <sup>b</sup>Conversion (%) and selectivity (%) were determined by GC–MS on an SE-54 column. <sup>c</sup>Fifth cycle, and the byproduct is 1-phenylethanol.

small sizes, thus allowing much higher catalytic performance than in the case of larger substrates. The latter molecules have difficulty entering the interior pore spaces, and reactions can only occur at exterior solid surfaces.

Immobilization of POM polyanions results in high selectivity and reactivity than single POM polyanions and MOF. It is likely that electrostatic interactions between the solvent accessible Cu(II) centers of the MOF structure and the encapsulated [PMo<sub>12</sub>O<sub>40</sub>]<sup>3–</sup> units are present in HLJU–1, and these stabilize HLJU–1 relative to its components. Such electrostatic POM–MOF interactions could simultaneously increase the rates of the substrate oxidation [PMo<sub>12</sub>O<sub>40</sub>]<sup>3–</sup> reduction step in the overall oxidations catalyzed by the POM@MOF. It is speculated that the mechanism of the catalytic reaction inside the pores of HLJU–1 involves multiple steps and the proposed mechanism, which are list in supporting information (see Scheme S1).

The toxicities of dyes have brought about a significant threat to the aqueous environment and caused serious consequences, such as aesthetic pollution, even carcinogenicity and perturbation to aquatic life. Nevertheless, most dyestuffs are difficult to degrade because of their stability to light and oxidants<sup>57</sup>. MOFs and POMs have been extensively indagated for adsorption and degradation dye molecules<sup>58–62</sup>. However, MOFs and POMs exhibit several weak points: for MOFs, the relative low stability in solution and brittleness or lack of flexibility; for POMs, feasible dissolution in water or polar organic liquids and relatively low surface area, which hampering their realistic applications. Recently, there have been two reports involved in the use of POM@MOFs composite as dyes adsorbent in Wang's group and Yang's group, which indicated that the combination of POM@MOFs

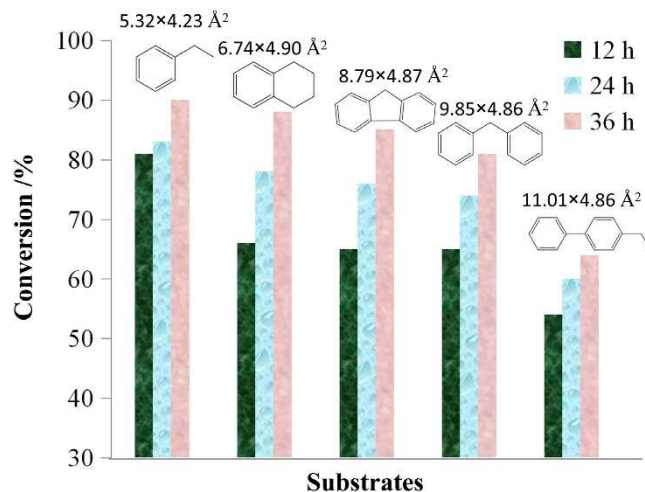


**Figure 4.** Conversions of oxidation reactions of alkylbenzenes with different sizes for the formation of phenylketones. Catalyst (0.005 mmol), alkylbenzene (1 mmol) and TBHP (5 mmol) were stirred at 80 °C for 12 h, 24 h and 36 h. Conversions are based on GC analysis. The molecular size of substrate is indicated at the top of each column.

could overcome the defects of each component<sup>65,66</sup>. Then HLJU 1–3 are applied to remove dyes from aqueous solutions. To contrast the adsorption activity of rht-MOF-1 and HLJU 1–3, the UV/visible absorption spectra of rhodamine B and crystal violet solution in the presence of rht-MOF-1 and HLJU 1–3 were conducted, respectively. As shown in Fig. 5, the uptake capacity of the HLJU 1–3 are obviously higher than that for rht-MOF-1. It is attributed to effect of the charges from the POM polyoxoanions on the uptake capacity. While the uptake capacity of the HLJU-2 is obviously higher than that for HLJU-1 and HLJU-3, attributing to that the electron charge of polyoxoanions  $\text{SiMo}_{12}^{4-}$  in HLJU-2 is more than those of  $\text{PMo}_{12}^{3-}$  and  $\text{PW}_{12}^{3-}$  in HLJU-1 and HLJU-3 respectively. This result indicates that the more negative charges the more uptake capacity. It is worth to note that the crystal violet uptake capacity of HLJU-2 (0.093  $\text{mmol}\cdot\text{g}^{-1}$ ) is much higher than that of  $\{[\text{Cd}(\text{DMF})_2\text{-Mn}^{\text{III}}(\text{DMF})_2\text{TPyP}](\text{PW}_{12}\text{O}_{40})\}\cdot 2\text{DMF}\cdot 5\text{H}_2\text{O}$  (0.057  $\text{mmol}\cdot\text{g}^{-1}$ ), a layered POM-Mn<sup>III</sup>-metalloporphyrin-based hybrid material<sup>36</sup>. The rhodamine B uptake capacity of HLJU-2 (10  $\text{mmol}\cdot\text{g}^{-1}$ ) is higher than that of  $\text{H}_6\text{P}_2\text{W}_{18}\text{O}_{62}\text{@MOF-5}$  (9  $\text{mmol}\cdot\text{g}^{-1}$ ) and lower than that of  $\text{PW}_{11}\text{V@MIL-101}$  (40  $\text{mmol}\cdot\text{g}^{-1}$ )<sup>63,64</sup>. The adsorption of the rhodamine B occurs in the open channels, which lead to the higher uptake capacity of  $\text{PW}_{11}\text{V@MIL-101}$ . Since the size of windows in HLJU 1–3 (5.9 Å) is much smaller than the diameters of the dyes (10.8 Å for rhodamine B and 13.2 Å for crystal violet), it can be concluded that the adsorption of the dyes occurs on the solid surfaces.

## Conclusions

Isolation of POM@MOF HLJU 1–3 first demonstrates that the Keggin POMs can be immobilized into the  $\beta$ -cage of rht-MOF-1 by a solvothermal method with highly ordered and porous structure. The highly ordered structure results in the well dispersion of POMs that synergistically promote the catalytic oxidation activity of alkylbenzenes, while highly porous structure with plentiful POM polyoxoanions enhance the adsorption efficiency for RhB and crystal violet dyes. Significantly, various pore dimensions in HLJU 1–3 afford an opportunity for selection of substrates in the catalytic reactions. This approach may inspire the study on immobilization of POMs into various MOFs to construct functional porous frameworks as heterogeneous catalysts and pollutants scavenger.

## Methods

**Synthesis of HLJU 1–3.** A solution of  $\text{CuCl}_2\cdot 2\text{H}_2\text{O}$  (0.03 g, 0.18 mmol), 5-tetrazolyisophthalic acid ( $\text{H}_3\text{TZI}$ ) (0.011 g, 0.047 mmol) and  $\text{H}_3\text{PMo}_{12}\text{O}_{40}\cdot n\text{H}_2\text{O}$  (0.1 g, 0.055 mmol) for HLJU-1,  $\text{H}_3\text{SiMo}_{12}\text{O}_{40}\cdot n\text{H}_2\text{O}$  (0.1 g, 0.055 mmol) for HLJU-2, and  $\text{H}_4\text{PW}_{12}\text{O}_{40}\cdot n\text{H}_2\text{O}$  (0.1 g, 0.035 mmol) for HLJU-3 in 1 mL of *N,N*-dimethylformamide (DMF) and 1 mL of distilled water was heated to 85 °C for 12 h, followed by slow cooling to room temperature. Blue or green octahedral crystals of HLJU 1–3 were then collected. The entire yields for HLJU 1–3: 60–80% based on Cu. IR (KBr,  $\text{cm}^{-1}$ ) for HLJU-1: 1626(s), 1566(s), 1438(s), 1387(s), 1273(w), 1048(w), 942(m), 870(m), 808(m), 752(w); for HLJU-2: 1646(s), 1570(s), 1435(s), 1387(s), 1251(w), 1108(m), 957(s), 905(m), 784(s), 751(s), 731(s); for HLJU-3: 1651(s), 1566(s), 1501(s), 1436(s), 1389(s), 1250(w), 1101(m), 1059(m), 956(m), 884(w), 811(w), 751(s), 733(s). Elemental Anal. Calcd (Found %) for  $\text{C}_{108}\text{H}_{171}\text{N}_{48}\text{Cu}_{24}\text{PMo}_{12}\text{O}_{160}$  (7409.10)(HLJU-1): C, 17.51(17.53); H, 2.33(2.36); N, 9.07(9.09); for  $\text{C}_{108}\text{H}_{172}\text{N}_{48}\text{Cu}_{24}\text{SiMo}_{12}\text{O}_{160}$  (7407.22)(HLJU-2): C, 17.51(17.54); H, 2.34(2.38); N, 9.08(9.11); for  $\text{C}_{108}\text{H}_{147}\text{N}_{48}\text{Cu}_{24}\text{PW}_{12}\text{O}_{148}$  (8247.72)(HLJU-3): C, 15.73(17.75); H, 1.80(1.83); N, 8.15(8.18).

**Crystal data for HLJU-1.** (CCDC no. 1058671):  $\text{C}_{108}\text{H}_{171}\text{N}_{48}\text{Cu}_{24}\text{PMo}_{12}\text{O}_{160}$ ,  $M = 7409.10$ , cubic,  $a = b = c = 44.599(3)$  Å,  $\alpha = \beta = \gamma = 90.00^\circ$ ,  $V = 88712(18)$  Å<sup>3</sup>,  $T = 293(2)$  K, space group  $Fm\bar{3}m$ ,  $Z = 8$ , 18345

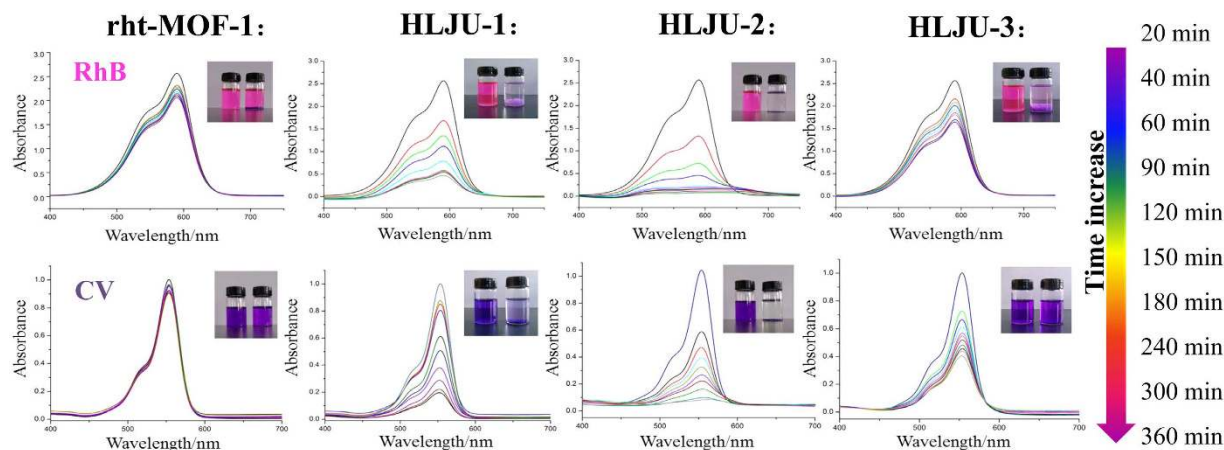


**Figure 5.** (top) UV–vis spectra of rhodamine B after the addition of solid rht-MOF-1 and HLJU 1–3 as time increase. (bottom) UV–vis spectra of crystal violet after the addition of solid rht-MOF-1 and HLJU 1–3 as time increase. The inset photographs highlight the scavenging effects.

reflections measured. The final  $R_1$  values were 0.0875 ( $I > 2\sigma(I)$ ). The final  $wR$  ( $F^2$ ) values were 0.2584 ( $I > 2\sigma(I)$ ). The final  $R_1$  values were 0.0997 (all data). The final  $wR$  ( $F^2$ ) values were 0.2696 (all data).

**Crystal data for HLJU-2.** (CCDC no. 1058599):  $C_{108}H_{172}N_{48}Cu_{24}SiMo_{12}O_{160}$ ,  $M = 7407.22$ , cubic,  $a = b = c = 44.614(5)$  Å,  $\alpha = \beta = \gamma = 90.00^\circ$ ,  $V = 88800(30)$  Å<sup>3</sup>,  $T = 293(2)$  K, space group  $Fm\bar{3}m$ ,  $Z = 8$ , 16911 reflections measured. The final  $R_1$  values were 0.0710 ( $I > 2\sigma(I)$ ). The final  $wR$  ( $F^2$ ) values were 0.2017 ( $I > 2\sigma(I)$ ). The final  $R_1$  values were 0.0967 (all data). The final  $wR$  ( $F^2$ ) values were 0.2188 (all data).

**Crystal data for HLJU-3.** (CCDC no. 1058600):  $C_{108}H_{147}N_{48}Cu_{24}PW_{12}O_{148}$ ,  $M = 8247.72$ , cubic,  $a = b = c = 44.742(7)$  Å,  $\alpha = \beta = \gamma = 90.00^\circ$ ,  $V = 87968(4)$  Å<sup>3</sup>,  $T = 293(2)$  K, space group  $Fm\bar{3}m$ ,  $Z = 8$ , 3470 reflections measured. The final  $R_1$  values were 0.0994 ( $I > 2\sigma(I)$ ). The final  $wR$  ( $F^2$ ) values were 0.2314 ( $I > 2\sigma(I)$ ). The final  $R_1$  values were 0.1302 (all data). The final  $wR$  ( $F^2$ ) values were 0.2547 (all data).

**Characterization.** All of the chemicals were obtained from commercial sources and used without further purification. Elemental (C, H and N) analyses were performed on a Perkin-Elmer 2400 analyzer. FT-IR data were collected on a Perkin-Elmer 100 spectrophotometer by using KBr pellets in the range of 4500–450  $cm^{-1}$ . Thermal analyses were carried out on a STA-6000 with a heating rate of 10 °C  $min^{-1}$  in a temperature range from 30 °C to 800 °C in atmosphere. Powder X-ray diffraction (PXRD) data were recorded on a Rigaku D/Max-3B X-ray diffractometer with  $CuK\alpha$  as the radiation source ( $\lambda = 0.15406$  nm) in the angular range  $\theta = 5–50^\circ$  at room temperature. GC–MS spectra were recorded on a SHIMADZU GCMS-QP2010. Nuclear magnetic resonance (NMR) was carried out on a Bruker AVANCE III 500 system. The concentration of dyes was analyzed by a UV-visible spectrophotometer (Perkin-Elmer 35), which recorded the temporal UV-visible spectral variations of the dyes with characteristics absorbance peak. Electron paramagnetic resonance (EPR) spectra were recorded on a EMX-10/12 spectrometer.

**Typical procedure for oxidation of alkylbenzenes.** Oxidation reactions were performed for six alkylbenzenes: methylbenzene, ethylbenzene, fluorine, tetrahydronaphthalene, biphenyl methane, and 4-ethyl-1,1'-biphenyl. In a typical reaction, ethylbenzene (1 mmol), TBHP (5 mmol), and catalyst (0.005 mmol) were allowed to stir at 80 °C for 12 h. The conversion and selectivity were obtained by GC analysis using a capillary SE-54 column with a flame ionization detector (FID). After the reaction, the catalyst was separated by filtration subjected to a recycling experiment after full washing and heated at 100 °C for 6 h under vacuum.

**Dye Adsorption Experiment.** For Rhodamine B: adsorbent (50 mg) was added into a 50 mL aqueous solution of rhodamine B (9.5  $mg \cdot L^{-1}$ ) under stirring at room temperature. After 30 min, the solution was centrifuged, and the plasma was analyzed by UV-vis absorption spectroscopy. The amount of adsorbed dyes was calculated (Eq. 1).

$$Q_{ad} = \frac{(c_0 - c_{ad})V}{m} \quad (1)$$

where  $Q_{ad}$  (mmol/g) is the amount of adsorbed dyes by adsorbent **1**,  $C_0$  is the initial concentration of dyes in the water (mmol/L),  $C_{ad}$  is the concentration of dyes after adsorption (mmol/L),  $V$  is the volume of the solution (L), and  $m$  is the mass of adsorbent **1** (g).

For crystal violet: adsorbent (50 mg) was added into a 50 mL aqueous solution of crystal violet (15 mg·L<sup>-1</sup>) under stirring at room temperature. After 30 min, the solution was centrifuged, and the plasma was analyzed by UV-vis absorption spectroscopy.

## References

- Katsoulis, D. E. A survey of applications of polyoxometalates. *Chem. Rev.* **98**, 359–388 (1998).
- Müller, A., Peters, F., Pope, M. T. & Gatteschi, D. Polyoxometalates: very large clusters/nanoscale magnets. *Chem. Rev.* **98**, 239–272 (1998).
- Dolbecq, A., Dumas, E., Mayer, C. R. & Mialane, P. Hybrid organic-inorganic polyoxometalate compounds: from structural diversity to applications. *Chem. Rev.* **110**, 6009–6048 (2010).
- Mitchell, S. G. et al. Face-directed self-assembly of an electronically active archimedean polyoxometalate architecture. *Nat. Chem.* **2**, 308–312 (2010).
- Niu, J. et al. Organodiphosphonate-functionalized lanthanopolyoxomolybdate cages. *Chem. Eur. J.* **18**, 6759–6762 (2012).
- Zhang, Z. M. et al. A polyoxometalate-based single-molecule magnet with a mixed-valent {Mn(IV)<sub>2</sub>Mn(III)<sub>6</sub>Mn(II)<sub>4</sub>} core. *Chem. Commun.* **49**, 2515–2517 (2013).
- Rhule, J. T., Hill, C. L., Judd, D. A. & Schinazi, R. F. Polyoxometalated in medicine. *Chem. Rev.* **98**, 327–358 (1998).
- Kikukawa, Y. et al. Synthesis and catalysis of di- and teranuclear metal sandwich-type silicotungstates [( $\gamma$ -SiW<sub>10</sub>O<sub>36</sub>)<sub>2</sub>M<sub>2</sub>( $\mu$ -OH)<sub>2</sub>]<sup>10-</sup> and [( $\gamma$ -SiW<sub>10</sub>O<sub>36</sub>)<sub>2</sub>M<sub>4</sub>( $\mu$ -O)( $\mu$ -OH)<sub>6</sub>]<sup>8-</sup> (M=Zr or Hf). *J. Am. Chem. Soc.* **130**, 5472–5478 (2008).
- Kuang, X. et al. Assembly of a metal-organic framework by sextuple intercatenation of discrete adamantane-like cages. *Nat. Chem.* **2**, 461–465 (2010).
- Zheng, S. T., Zhang, J., Clemente-Juan, J. M., Yuan, D. Q. & Yang, G. Y. Cheminform abstract: poly(polyoxotungstate)s with 20 Nickel centers: from nanoclusters to one-dimensional chains. *Angew. Chem. Int. Ed.* **48**, 7176–7179 (2009).
- Kozhevnikov, I. V. Catalysis by heteropoly acids and multicomponent polyoxometalated in liquid-phase reactions. *Chem. Rev.* **98**, 171–198 (1998).
- Chen, Y., Zhao, S. & Song, Y. F. An efficient heterogeneous catalyst based on highly dispersed Na<sub>7</sub>H<sub>2</sub>LaW<sub>10</sub>O<sub>36</sub>·32H<sub>2</sub>O nanoparticles on mesoporous silica for deep desulfurization. *Appl. Catal. A* **466**, 307–314 (2013).
- Sousa, J. L. C. et al. Iron(III)-substituted polyoxotungstates immobilized on silica nanoparticles: novel oxidative heterogeneous catalysts. *Catal. Commun.* **12**, 459–463 (2011).
- Alcañiz-Monge, J., Trautwein, G., Parres-Esclapez, S. & Maciá-Agulló, J. A. Influence of microporosity of activated carbons as a support of polyoxometalates. *Micropor. Mesopor. Mater.* **115**, 440–446 (2008).
- Ruiz, V., Suárez-Guevara, J. & Gomez-Romero, P. Hybrid electrodes based on polyoxometalate-carbon materials for electrochemical supercapacitors. *Electrochem. Commun.* **24**, 35–38 (2012).
- Yan, D. P., Tang, Y. Q., Lin, H. Y. & Wang, D. Tunable two-color luminescence and host-guest energy transfer of fluorescent chromophores encapsulated in metal-organic frameworks. *Sci. Rep.* **4**, 4337 (2014).
- Long, J. R. & Yaghi, O. M. The pervasive chemistry of metal-organic frameworks. *Chem. Soc. Rev.* **38**, 1213–1214 (2009).
- Tranchemontagne, D. J., Mendoza-Cortes, J. L., O’Keeffe, M. & Yaghi, O. M. Secondary building units, nets and bonding in the chemistry of metal-organic frameworks. *Chem. Soc. Rev.* **38**, 1257–1283 (2009).
- O’Keeffe, M., Peskov, M. A., Ramsden, S. J. & Yaghi, O. M. The reticular chemistry structure resource (RCSR) database of, and symbols for, crystal nets. *Acc. Chem. Res.* **41**, 1782–1789 (2008).
- Ockwig, N. W., Delgado-Friedrichs, O., O’Keeffe, M. & Yaghi, O. M. Reticular chemistry: occurrence and taxonomy of nets and grammar for the design of frameworks. *Acc. Chem. Res.* **38**, 176–182 (2005).
- Eddaoudi, M. et al. Modular chemistry: secondary building units as a basis for the design of highly porous and robust metal-organic carboxylate frameworks. *Acc. Chem. Res.* **34**, 319–330 (2001).
- Yaghi, O. M., Li, H., Davis, C., Richardson, D. & Groy, T. L. Synthetic strategies, structure patterns, and emerging properties in the chemistry of modular porous solids. *Acc. Chem. Res.* **31**, 474–484 (1998).
- Czaja, A. U., Trukhan, N. & Muller, U. Industrial applications of metal-organic frameworks. *Chem. Soc. Rev.* **38**, 1284–1293 (2009).
- Zheng, S. T., Zhang, J. & Yang, G. Y. Designed synthesis of POM-organic frameworks from {Ni<sub>6</sub>PW<sub>6</sub>} building blocks under hydrothermal conditions. *Angew. Chem. Int. Ed.* **47**, 3909–3913 (2008).
- Corma, A. & García, H. & Llabrés i Xamena, F. X. Engineering metal organic frameworks for heterogeneous catalysis. *Chem. Rev.* **110**, 4606–4655 (2010).
- Ma, L., Abney, C. & Lin, W. Enantioselective catalysis with homochiral metal-organic frameworks. *Chem. Soc. Rev.* **38**, 1248–1256 (2009).
- Férey, G. Hybrid porous solids: past, present, future. *Chem. Soc. Rev.* **37**, 191–214 (2008).
- Eddaoudi, M. et al. Systematic design of pore size and functionality in isorectical MOFs and their application in methane storage. *Science* **295**, 469–472 (2002).
- Murray, L. J., Dinca, M. & Long, J. R. Hydrogen storage in metal-organic frameworks. *Chem. Soc. Rev.* **38**, 1294–1314 (2009).
- Sun, C.-Y. et al. Highly stable crystalline catalysts based on a microporous metal-organic framework and polyoxometalates. *J. Am. Chem. Soc.* **131**, 1883–1888 (2009).
- Bajpe, S. R. et al. Direct observation of molecular-level template action leading to self-assembly of a porous framework. *Chem. Eur. J.* **16**, 3926–3932 (2010).
- Song, J. et al. A multiunit catalyst with synergistic stability and reactivity: a polyoxometalate-metal organic framework for aerobic decontamination. *J. Am. Chem. Soc.* **133**, 16839–16846 (2011).
- Han, Q. et al. Engineering chiral polyoxometalate hybrid metal-organic frameworks for asymmetric dihydroxylation of olefins. *J. Am. Chem. Soc.* **135**, 10186–10189 (2013).
- Dey, C. & Banerjee, R. Controlled synthesis of a catalytically active hybrid metal-oxide incorporated zeolitic imidazolate framework (MOZIF). *Chem. Commun.* **49**, 6617–6619 (2013).
- Canoni, R. et al. Stable polyoxometalate insertion within the mesoporous metal organic framework MIL-100(Fe). *J. Mater. Chem.* **21**, 1226–1233 (2011).
- Zou, C. et al. A multifunctional organic-inorganic hybrid structure based on Mn(III)-prophyrin and polyoxometalate as a highly effective dye scavenger and heterogeneous catalyst. *J. Am. Chem. Soc.* **134**, 87–90 (2012).
- Yang, L., Naruke, H. & Yamase, T. A novel organic/inorganic hybrid nanoporous material incorporating Keggin-type polyoxometalates. *Inorg. Chem. Commun.* **6**, 1020–1024 (2003).
- Salomon, W. et al. Immobilization of polyoxometalates in the Zr-based metal organic framework UIO-67. *Chem. Commun.* **51**, 2972–2975 (2015).
- Férey, G. et al. Erratum: a chromium terephthalate-based solid with unusually large pore volumes and surface area. *Science* **309**, 2040–2042 (2005).
- Maksimchuk, N. V., Kholdeeva, O. A., Kovalenko, K. A. & Fedin, V. P. MIL-101 supported polyoxometalates: synthesis, characterization, and catalytic applications in selective liquid-phase oxidation. *Isr. J. Chem.* **51**, 281–289 (2011).
- Maksimchuk, N. V. et al. Heterogeneous selective oxidation catalysts based on coordination polymer MIL-101 and transition metal-substituted polyoxometalates. *J. Catal.* **257**, 315–323 (2008).

42. Maksimchuk, N. V. *et al.* Hybrid polyoxotungstate/MIL-101 materials: synthesis, characterization, and catalysis of H<sub>2</sub>O<sub>2</sub>-based alkene epoxidation. *Inorg. Chem.* **49**, 2920–2930 (2010).
43. Ribeiro, S. *et al.* An efficient oxidative desulfurization process using terbium-polyoxometalate@MIL-101(Cr). *Catal. Sci. Technol.* **3**, 2404–2414 (2013).
44. Balula, S. S., Granadeiro, C. M., Barbosa, A. D. S., Santos, I. C. M. S. & Cunha-Silva, L. Multifunctional catalyst based on sandwich-type polyoxotungstate and MIL-101 for liquid phase oxidations. *Catal. Today* **210**, 142–148 (2013).
45. Chui, S. S.-Y., Lo, S. M.-F., Charmant, J. P. H., Orpen, A. G. & Williams, I. D. A chemically functionalizable nanoporous material [Cu<sub>3</sub>(TMA)<sub>2</sub>(H<sub>2</sub>O)<sub>3</sub>]<sub>n</sub>. *Science* **283**, 1148–1150 (1999).
46. Wee, L. H. *et al.* Convenient synthesis of Cu<sub>3</sub>(BTC)<sub>2</sub> encapsulated Keggin heteropolyacid nanomaterial for application in catalysis. *Chem. Commun.* **46**, 8186–8188 (2010).
47. Ma, F. J. *et al.* A sodalite-type porous metal-organic framework with polyoxometalate templates: adsorption and decomposition of dimethyl methylphosphonate. *J. Am. Chem. Soc.* **133**, 4178–4181 (2011).
48. Juan-Alcañiz, J. *et al.* Live encapsulation of a Keggin polyanion in NH<sub>2</sub>-MIL-101(Al) observed by *in situ* time resolved X-ray scattering. *Chem. Commun.* **47**, 8578–8580 (2011).
49. Bromberg, L., Diao, Y., Wu, H. M., Speakman, S. A. & Hatton, T. A. Chromium(III) terephthalate metal organic framework (MIL-101): HF-free synthesis, structure, polyoxometalate composites, and catalytic properties. *Chem. Mater.* **24**, 1664–1675 (2012).
50. Zhang, Y. M., Degirmenci, V., Li, C. & Hensen, E. J. M. Phosphotungstic acid encapsulated in metal-organic framework as catalysts for carbohydrate dehydration to 5-hydroxymethylfurfural. *ChemSusChem* **4**, 59–64 (2011).
51. Eubank, J. F. *et al.* On demand: the singular rht net, an ideal blueprint for the construction of a metal-organic framework(MOF) platform. *Angew. Chem. Int. Ed.* **51**, 10099–10103 (2012).
52. Nouar, F. *et al.* Supermolecular building blocks (SBBs) for the design and synthesis of highly porous metal-organic frameworks. *J. Am. Chem. Soc.* **130**, 1833–1835 (2008).
53. Farrugia, L. WinGX suite for small-molecule single-crystal crystallography. *J. Appl. Cryst.* **32**, 837–838 (1999).
54. Sheldrick, G. M. Phase annealing in SHELX-90: direct methods for larger structures. *Acta Cryst. A* **46**, 467–473 (1990).
55. Sheldrick, G. M. A short history of SHELX. *Acta Cryst. A* **64**, 112–122 (2008).
56. Furukawa, H. *et al.* Oxidation of cyclopentene with hydrogen peroxide catalyzed by 12-heteropoly acids. *Chem. Lett.* **5**, 877–880 (1988).
57. Chen, S. H. *et al.* Equilibrium and kinetic studies of methyl orange and methyl violet adsorption on activated carbon derived from *Phragmites australis*. *Desalination* **252**, 149–156 (2010).
58. Yi, F.-Y. *et al.* Polyoxometalates-based heterometallic organic-inorganic hybrid materials for rapid adsorption and selective separation of methylene blue from aqueous solutions. *Chem. Commun.* **51**, 3336–3339 (2015).
59. Lin, S. *et al.* Adsorption behavior of metal-organic frameworks for methylene blue from aqueous solution. *Micropor. Mesopor. Mater.* **193**, 27–34 (2014).
60. Zhang, C. F. *et al.* A novel magnetic recyclable photocatalyst based on a core-shell metal-organic framework Fe<sub>3</sub>O<sub>4</sub>@MIL-100(Fe) for the decolorization of methylene blue dye. *J. Mater. Chem. A* **1**, 14329–14334 (2013).
61. Lan, Y.-Q., Jiang, H. L., Li, S. L. & Xu, Q. Mesoporous metal-organic frameworks with size-tunable cages: selective CO<sub>2</sub> uptake, encapsulation of Ln<sup>3+</sup> cations for luminescence, and column-chromatographic dye separation. *Adv. Mater.* **23**, 5015–5020 (2011).
62. Qin, J.-S. *et al.* A microporous anionic metal-organic framework for sensing luminescence of lanthanide(III) ions and selective absorption of dyes by ionic exchange. *Chem.-Eur. J.* **20**, 5625–5630 (2014).
63. Yan, A. X. *et al.* Incorporating polyoxometalates into a porous MOF greatly improves its selective adsorption of cationic dyes. *Chem. Eur. J.* **20**, 6927–6933 (2014).
64. Liu, X. X., Luo, J., Zhu, Y. T., Yang, Y. & Yang, S. J. Selective adsorption of cationic dyes from aqueous solution by polyoxometalate-based metal-organic framework composite. *Appl. Surf. Sci.* **362**, 517–524 (2016).

## Acknowledgements

This work is financially supported by the National Natural Science Foundation of China (Nos 21272061, 21502046, 21471051 & 51473046).

## Author Contributions

J.W.S. and J.Q.S. designed the research and wrote the paper, G.H.A. did the characterization and analysed the data, P.F.Y., G.M.L. and G.Y.Y. directed the research. All authors discussed the results and reviewed the manuscript.

## Additional Information

**Supplementary information** accompanies this paper at <http://www.nature.com/srep>

**Competing financial interests:** The authors declare no competing financial interests.

**How to cite this article:** Sun, J.-W. *et al.* Immobilization of Polyoxometalate in the Metal-Organic Framework rht-MOF-1: Towards a Highly Effective Heterogeneous Catalyst and Dye Scavenger. *Sci. Rep.* **6**, 25595; doi: 10.1038/srep25595 (2016).



This work is licensed under a Creative Commons Attribution 4.0 International License. The images or other third party material in this article are included in the article's Creative Commons license, unless indicated otherwise in the credit line; if the material is not included under the Creative Commons license, users will need to obtain permission from the license holder to reproduce the material. To view a copy of this license, visit <http://creativecommons.org/licenses/by/4.0/>